A Closure for the Virtual Origin of Turbulent Plumes

Nathaniel Tarshish *

Department of Earth and Planetary Science, University of California, Berkeley, California

David M. Romps

Department of Earth and Planetary Science, University of California, Berkeley, California, and Climate and Ecosystem Sciences Division, Lawrence Berkeley National Laboratory, Berkeley, California

ABSTRACT

An isolated source of surface buoyancy, be it a campfire or burning city, gives rise to a turbulent plume. Well above the surface, the plume properties asymptote to the well-known solutions of Morton, Taylor, and Turner (MTT), but a closure is still lacking for the virtual origin. A closure for the virtual origin is sought here in the case of a turbulent plume sustained by a circular source of surface buoyancy in an unstratified and unsheared fluid. In the high Reynolds number limit, it is argued that all such plumes asymptote to a single solution. Direct numerical simulation (DNS) of this solution exhibits a virtual origin located a distance below the surface equal to 1.1 times the radius of the buoyancy source. This solution is compared to the previously used assumption that the MTT plume is fully spun-up at the surface, and that assumption is found to give buoyancies that are off by an order of magnitude. With regards to the citywide firestorm triggered by the nuclear attack on Hiroshima, it is found that the spun-up-at-surface MTT solution would have trapped radioactive soot within about a hundred meters of the surface, whereas the DNS solution presented here corroborates observations of the plume reaching well into the troposphere.

1. Introduction

In the presence of gravity, a steady isolated heating at the bottom of an unstratified fluid will produce a plume: a buoyant column of rising fluid whose steady shape is maintained (in spite of its ascent) by the entrainment of surrounding fluid. A pleasant and familiar example is the turbulent and smoky plume generated by a campfire. A decidedly less pleasant example is the plume generated by a city-sized fire ignited by a nuclear weapon. This latter case, with its attendant threat of stratospheric soot injection and climate perturbation, motivates the objective of this paper: to characterize the near-surface spin-up of such plumes.

For the sake of simplicity, we focus here on buoyancy-driven plumes in an unstratified fluid initially at rest, or in cases where the background flow is small enough to have a negligible effect on the plume's gross characteristics. Aside from the surface fire, we assume there are no diabatic sources of heat. In the atmosphere, this means that the air is taken to be dry, i.e., we focus on the dynamics of plumes below their lifting condensation level.

Morton et al. (1956) (hereafter, MTT) established the foundational closure for plumes far from their source of buoyancy in a neutral Boussinesq fluid: by dimensional analysis, MTT postulated that the plume's turbulent mixing length is proportional to the plume's width. As reviewed in Turner (1986), numerous experiments in the laboratory (Carazzo et al. 2006), flows in nature (Woods 2010), and numerical simulations (Devenish et al. 2010) have tested the MTT theory and found close agreement. Subsequent work has built on this foundation, analyzing plumes in more complex settings, such as non-Boussinesq fluids (Rooney and Linden 1996) and stratified environments (Woods 2010).

For many applications, motion far above the source is of primary interest (e.g., Carazzo et al. 2006, Table 1). Near the source, however, the flow is manifestly different from the canonical MTT plume: a horizontal circulation converges fluid over the source, mixes in environmental air, and launches the fluid upward. If we wish to predict the fate of the buoyant fluid (e.g., its eventual level of neutral buoyancy), we must be able to predict the height at which the plume has largely transitioned to an MTT regime, as well as the plume's buoyancy, width, and vertical velocity at that height.

At present, there is no rigorous theory for the near-surface dynamics of buoyancy-driven plumes. Indeed, our search of the literature turned up neither empirical data on nor well-resolved simulations of the near-surface flow in response to an isolated heating at a no-slip lower boundary. Absent the requisite data or theory for the spin-up layer, some researchers have resorted to the ad hoc practice of initializing the MTT plume as fully spun-up at the surface with the full radius of the source (Freitas et al.

*Corresponding author: Nathaniel Tarshish, tarshish@berkeley.edu

2007; Paugam et al. 2016) while others have neglected the source's radius entirely (Penner et al. 1986; Carrier et al. 1985; Manins 1985), modeling the plume's source as point-like at the surface. By neglecting the spin-up boundary layer entirely, both of these initializations have the non-physical consequence of $w \neq 0$ at the surface — a mismatch that may play a role in why wildfire plume predictions compare poorly to observations (Paugam et al. 2016).

In the MTT solution, the turbulent plume has the shape of a cone. At the vertex of the cone, the radius of the plume is zero and the buoyancy and vertical velocity are infinite. Of course, no plume in reality has such a vertex, but real plumes (in unstratified, unsheared fluids) do asymptote to the MTT solution sufficiently far above their heating source. At those heights, the plume is fully characterized by only two quantities: the buoyancy source rate and the location of the vertex of the best-fit cone, which is called the virtual origin. The two ad hoc initializations described above differ only in their choice of virtual origin. When initializing a plume as emanating from a point at the surface, the height of the virtual origin z_v is zero. For the spun-up-at-surface plume, whose width at the surface equals the width of the surface buoyancy source, $z_v < 0$. In either case, however, the only other parameter – the buoyancy source rate – is set to the actual rate. Therefore, to model real plumes far above the surface, what is needed is a closure for the virtual origin.

Although a great number of papers have been written about plumes, we were unable to find any closure in the literature for the virtual origin of a plume with the following three properties relevant to real-world fires: a plume that has 1. well-resolved turbulence and that is 2. sourced only by buoyancy at a 3. no-slip surface. To fill that gap, we present here a closure for the virtual origin of such plumes using direct numerical simulations in two and three dimensions. To illustrate the importance of using the correct virtual origin, we will estimate the level of neutral buoyancy of the Hiroshima nuclear firestorm plume using the new closure and, for comparison, the commonly used spun-up-at-surface closure. Before we begin, however, let us briefly review some of the prior literature to see the ways in which conditions 1, 2, and 3 have been missing from previous studies.

Two theoretical predictions have been made for the virtual origin of a plume driven by a circular source of buoyancy. Those calculations used turbulence closures to derive analytic solutions for a buoyancy-driven plume that is initialized by a finite-area circular source rather than a point source (as is the case for the MTT plume). The turbulence closure adopted by Hunt and Kaye (2001) modeled the plume's fractional entrainment rate as α/r, where r is the plume's radius and α is the same dimensionless constant found empirically for far-field plumes (see the discussion of α in section 2). That closure leads to an analytic solution with a virtual origin at the same height as the circular source of buoyancy. Ciriello and Hunt (2020) replaced α with a linear function of the plume's Richardson number and found an analytic solution (their $\Gamma_0 \to \infty$ solution) in which the virtual origin is located below the physical source of buoyancy by a distance of about 3.34 times the physical source's radius. The accuracy of these predictions is uncertain given their dependence on simplified approximations of the plume dynamics.

Three types of empirical approaches have been dominant in plume studies: water-tank experiments, heated-air experiments, and numerical simulations. In the water-tank experiments (Colomer et al. 1999; Friedl et al. 1999; Epstein and Burelbach 2001; Kaye and Hunt 2009), it has been common to pump salty water into a fresh water tank, initializing the near-source fluid with both mass and momentum in addition to buoyancy, thereby violating condition 2. Compounding the problem, few eddies were present in the above experimental near-source flows (see Figures 1 and 2 of Kaye and Hunt 2009) suggesting laminar growth (Friedl et al. 1999). Therefore, these water-tank experiments do not satisfy conditions 1 and 2.

In the heated-air experiments, the plumes are typically generated by a heated metal disk. However, the majority of these studies placed the disk atop a cylinder (e.g., Bouzinaoui et al. 2007; Fontaine et al. 2006; Vuong Pham et al. 2005; Popiolek et al. 1998; Elicer-CortÃŕs 1998; Kofoed and Nielsen 1990), producing a free-slip flow rather than condition 3 of a no-slip surface. Kuznetsov et al. (2019) and Mahmoud et al. (2009) enforced the no-slip boundary condition by heating metal disks embedded in a lower surface, but these studies did not compute the virtual origin nor present data from which the virtual origin can be inferred.

Numerical simulations have also investigated plumes evolving from a circular heat source (Devenish et al. 2010; Fontaine et al. 2006; Plourde et al. 2008). The large-eddy simulations of Devenish et al. (2010) used a horizontal resolution that was appropriate for the far-field dynamics, but coarse compared to the source's width, and so did not meet condition 1 of having well-resolved turbulence. The simulated plume of Fontaine et al. (2006) had a free-slip elevated source and so did not meet condition 3. Finally, Plourde et al. (2008) performed higher-resolution simulations of a plume fed by a circular source of buoyancy at a no-slip surface, but found an "unrealistically laminar" plume, which was then made to be approximately turbulent by continuously adding white noise to the near-surface vertical velocity. This suggests that, despite the high reported Reynolds number of 3055, this simulation did not satisfy condition 1 of having well-resolved turbulence. Furthermore, Plourde et al. (2008) reported that the "disturbance added to the flow close to the heat source is an important parameter that controls the onset and location of transition

[from a laminar to a turbulent state]". In section 3, we argue that the resolution in Plourde et al. (2008) was not sufficient to directly resolve dissipation at the Kolmogorov microscale, which is required for a direct numerical simulation to perform properly.

2. Theory

In this section, we will review the Morten-Taylor-Turner (MTT) solutions, the sensitivity of those solutions to the virtual origin, and the high-Reynolds-number limit.

a. Review of MTT

Our results build on the foundational theory of convective plumes put forth by MTT, which we now review. MTT formulates bulk conservation equations for a plume's volume, momentum, and buoyancy fluxes in an unstratified Boussinesq fluid. In doing so, the environment is taken to have zero vertical momentum, and buoyancy is assumed to be the dominant force. In a neutrally buoyant fluid, the MTT equations read

$$\frac{d}{dz}\left(r^2 w\right) = 2 r u_e, \tag{1}$$

$$\frac{d}{dz}\left(r^2 w^2\right) = r^2 b, \tag{2}$$

$$r^2 w b = Q = \text{constant}, \tag{3}$$

where the plume is described by radius r, buoyancy b, and vertical velocity w. By convention, Q is the buoyancy source divided by a factor of π. Turbulent entrainment of environmental air into the plume is quantified by the entrainment velocity u_e.

The MTT turbulence closure is $u_e = \alpha w$ for some dimensionless constant α. This closure stems from the reasonable guess that the sizes and speeds of the eddies responsible for entrainment scale with the size and speed, respectively, of the plume itself. Given this closure, the equations admit an analytical solution for the case in which the buoyancy source is located at a point,

$$r = \frac{6\alpha}{5}(z - z_v), \tag{4}$$

$$w = \frac{5^{1/3}}{2\alpha^{1/3}} Q^{1/3} r^{-1/3} \tag{5}$$

$$b = \frac{2\alpha^{1/3}}{5^{1/3}} Q^{2/3} r^{-5/3}. \tag{6}$$

In this solution, the buoyancy source is located at $r = 0$ and $z = z_v$. This point is referred to as the virtual origin. Away from the surface, real plumes asymptote to an MTT solution (with Q set by the physical buoyancy source) but with a virtual origin that is, in general, not located at the surface. Geometrically, z_v marks the apex of the cone swept out by the plume far above the surface. While fundamental to the solution, the MTT theory does not predict z_v and does not attempt to describe the near-surface dynamics. In this respect, real plumes remain an unsolved problem: a closure is needed for the virtual origin.

b. The virtual origin

In laboratory and numerical studies, the virtual origin is fit ex post facto to experiments (e.g., Carazzo et al. 2006, and references therein). Table 1 collects prior measurements. The relevance of these past experiments to atmospheric plumes, however, is unclear, as no past experiment has satisfied conditions 1, 2, and 3 described above. Lacking solid experimental footing, predictive studies on atmospheric plumes have relied on the ad hoc practice of ignoring the spin-up layer altogether. Some authors assume the plume is fully spun-up at $z = 0$ with radius equal to the radius R of the patch of surface heating (usually taken to be a circle): enforcing this spun-up-at-surface condition on $r(z)$ requires that the virtual origin be placed at $z_v = -\frac{5R}{6\alpha} \approx -9\text{R}$ (Paugam et al. 2016; Freitas et al. 2007), given the canonical $\alpha \approx .1$ (Carazzo et al. 2006). Other authors make the ad hoc choice of placing the virtual origin at the surface by setting $z_v = 0$ (Penner et al. 1986; Carrier et al. 1985).

To determine whether these choices of z_v are consequential, we note that $b(z, z_v) \propto (z - z_v)^{-5/3}$ and compute the ratio,

$$\frac{b(z, z_v = 0)}{b(z, z_v = -9R)} = \left(1 + \frac{9R}{z}\right)^{5/3}. \tag{7}$$

If we are interested in the plume's buoyancy at heights comparable to the horizontal extent of the buoyancy source, then we could plug $z = R$ into this expression. This yields a buoyancy ratio of 46. Thus, the choice of initialization has immense consequences for the plume's height of neutral buoyancy and, in the case of an urban firestorm, how much climate-altering soot reaches the upper atmosphere. If the virtual origin is not particularly sensitive to relaxing conditions 1, 2, and 3, then prior experimental work on related plumes is relevant, and suggests $z_v = 0$ is a more plausible assumption in light of the data in Table 1. Given the array of varied and conflicting initializations, we seek to definitively establish the plume's virtual origin for the case of interest with direct numerical simulations.

c. The turbulent limit

The success and broad applicability of the MTT theory rests on the observation that fully developed plumes appear to exhibit a nearly universal rate of change in radius with respect to height, independent of the experimental setup or fluid composition. This growth rate, captured by the entrainment rate α, is found to be close to 0.1 in a wide range of experiments (as reviewed in Carazzo et al. 2006).

	Type	Surface Fluxes	BC	Re	z_ν [R]
Devenish et al. (2010)	LES	Buoyancy	no slip	N/A	−1.4
Fontaine et al. (2006)	LES	Buoyancy	free slip	20000	−2.2 or −1.2
Plourde et al. (2008)	DNS	Buoyancy, Momentum Noise	no slip	N/A	−2.2
Bouzinaoui et al. (2007)	Heated air	Buoyancy	free slip	20000	−2
Kofoed and Nielsen (1990)	Heated air	Buoyancy	free slip	100	−.88
Elicer-CortÃĭs (1998)	Heated air	Buoyancy	free slip	800	−.86
Kaye and Hunt (2009)	Salt water	Buoyancy, Volume, Momentum	free slip	N/A	−2
Colomer et al. (1999)	Salt water	Buoyancy, Volume, Momentum	free slip	4000	−1.6
Ciriello and Hunt (2020)	Theory	Buoyancy-only limit	N/A	N/A	−3.34
Hunt and Kaye (2001)	Theory	Buoyancy-only limit	N/A	N/A	0.0

TABLE 1. Comparison of z_ν across prior work. See text for discussion. Fontaine et al. (2006) reports −2.2R and −1.2R for domain ventilation velocities of .15 m/s and .02 m/s, respectively. Least-squares fit to data in Figure 1 of Plourde et al. (2008) yields the reported z_ν. Since the simulation of Plourde et al. (2008) appears not to have been DNS, it is not possible to calculate its Reynolds number.

Scorer (1957), who first noted this invariance, hypothesized the existence of a universal self-similar solution that all plumes converge toward after turbulence dominates the flow.

For a neutral Boussinesq fluid, the flow is governed by the non-dimensional Reynolds number Re and the Prandtl number Pr, and Scorer's hypothesis implies that the large-scale features of the plume should converge to a single asymptote as Re increases, independent of Pr. Indeed, turbulent experiments with differing Pr (e.g., plumes in water versus air) demonstrate similar entrainment rates (Carazzo et al. 2006).

In this study, we perform direct numerical simulations that allow us to explicitly set the non-dimensional parameters and explore this high-Re convergence. To fix terms and define the non-dimensional parameters, we study plumes that are solutions to the Boussinesq equations for an unstratified, incompressible fluid,

$$\partial_t \mathbf{u} + (\mathbf{u}\cdot\nabla)\mathbf{u} = -\nabla\left(\frac{p'}{\rho_0}\right) + b\mathbf{e}_z + \nu\nabla^2\mathbf{u}, \tag{8}$$

$$\partial_t b + \mathbf{u}\cdot\nabla b = \kappa\nabla^2 b, \tag{9}$$

$$\nabla\cdot\mathbf{u} = 0, \tag{10}$$

where $\mathbf{u} = (u, v, w)$ is the velocity, ν is the kinematic viscosity, and κ is the thermal diffusivity. With a constant buoyancy flux F within radius R, the boundary conditions are

$$\mathbf{u}|_{z=0} = 0 \qquad \left.\frac{\partial b}{\partial z}\right|_{z=0} = \begin{cases} -F/\kappa & r \le R \\ 0 & r > R \end{cases}, \tag{11}$$

where $r = \sqrt{x^2+y^2}$. Casting the equations in non-dimensional form, we introduce dimensional scales $B = F^{2/3}R^{-1/3}$, $U = F^{1/3}R^{1/3}$, $T = F^{-1/3}R^{2/3}$, and $P = F^{2/3}R^{2/3}$. Denoting non-dimensional variables by a caret, we get

$$\partial_{\hat t}\hat{\mathbf{u}} + (\hat{\mathbf{u}}\cdot\hat\nabla)\hat{\mathbf{u}} = -\hat\nabla\hat p + \hat b\mathbf{e}_z + \frac{1}{\mathrm{Re}}\hat\nabla^2\hat{\mathbf{u}}, \tag{12}$$

$$\partial_{\hat t}\hat b + \hat{\mathbf{u}}\cdot\hat\nabla\hat b = \frac{1}{\mathrm{Re\,Pr}}\hat\nabla^2\hat b, \tag{13}$$

$$\hat{\mathbf{u}}|_{\hat z=0} = 0 \qquad \left.\frac{\partial\hat b}{\partial\hat z}\right|_{\hat z=0} = \begin{cases} -\mathrm{Re\,Pr} & \hat r \le 1 \\ 0 & \hat r > 1 \end{cases}, \tag{14}$$

where we have defined the Prandtl and Reynolds numbers as

$$\mathrm{Pr} = \frac{\nu}{\kappa}, \quad \mathrm{Re} = \frac{F^{1/3}R^{4/3}}{\nu}. \tag{15}$$

In this analysis, we take the atmospheric value of Pr = .7 and explore the solution's dependence on Re. Given the above non-dimensional equations, the non-dimensional solution is fully specified by the global Re and Pr. By dimensional reasoning, the plume's time-averaged center-line vertical velocity w_c and buoyancy b_c must take the forms $b_c = \hat b_c(\mathrm{Re},\mathrm{Pr},\hat z)F^{2/3}R^{-1/3}$ and $w_c = \hat w_c(\mathrm{Re},\mathrm{Pr},\hat z)F^{1/3}R^{1/3}$, where the non-dimensional scaling functions are at present unknown.

The global Re defined above is closely related to the plume's local Reynolds number $\mathrm{Re}_{\mathrm{local}}$ expressed in terms of the plume's vertical velocity w_c as

$$\mathrm{Re}_{\mathrm{local}} = \frac{w_c r}{\nu} = \mathrm{Re}\,\hat w_c\hat r = \frac{5^{1/3}}{2\alpha^{1/3}}\mathrm{Re}\,\hat r^{2/3}, \tag{16}$$

where we have applied the MTT scalings (Eqn. 5) and emphasize that the global Re is a constant fixed by the source's scales and the fluid's viscosity. We see that the plume's local Reynolds number increases as the plume rises and widens. Growth of the MTT plume, however, only explicitly depends on α, and laboratory experiments peg α to a height-independent constant value (Carazzo et al. 2006). The fact that α remains fixed at the universal value of approximately 0.1 as $\mathrm{Re}_{\mathrm{local}}$ increases is a consequence of the fluid flow having already asymptoted to the high-$\mathrm{Re}_{\mathrm{local}}$

limit. In what follows, we will show that this same asymptotic behavior applies not just to the far-field MTT plume, but also to the near-surface spin-up layer that initializes the plume.

3. Model

We solve the non-dimensionalized Boussinesq equations (Eqns. 12, 13, and 14) with Dedalus, a pseudo-spectral framework for direct numerical simulations (Burns et al. 2020). The simulation is run with Pr = .7 and Re = 10^3 in a cubic domain with side length 12 (recall that the equations have been non-dimensionalized). Two-dimensional simulations are run in an identical square domain at various Re. In the z-dimension, we express the fields as a Chebyshev series. At the surface, no-slip boundary conditions are enforced and a circular spectrally-smooth source of buoyancy is specified,

$$\left.\frac{\partial \hat{b}}{\partial \hat{z}}\right|_{\hat{z}=0} = -\frac{\mathrm{RePr}}{2}\left[1-\tanh\left(\frac{\sqrt{\hat{x}^2+\hat{y}^2}-1}{\Delta r}\right)\right], \qquad (17)$$

with $\Delta r = .01$. In the horizontal, the fields are expanded in Fourier series.

To be considered a direct numerical simulation, the spectral modes, when projected onto a collocation grid in physical space, must satisfy the requirement that the grid spacing Δx is $\mathrm{O}(\eta)$ where η is the Kolmogorov length (Moin and Mahesh 1998). In turn, η may be solved for by noting that the the length-scale of energy injection R is linked to the dissipation scale η via the Kolmogorov scaling $\eta/R = \mathrm{Re}^{-3/4}$. Setting Re = 10^3 and expanding the fields horizontally in $N = 512$ Fourier modes in Dedalus yields a physical space collocation grid with uniform horizontal resolution $\Delta x = \Delta y = 12R/512 \approx 4\eta$.

For the vertical Chebyshev basis, the collocation grid has variable resolution with a higher density of grid points near the surface. Grid points satisfying $z < R$ have an average grid spacing of $\Delta z \approx 1.1\eta$. The resolution of the surface flow thus meets the $\mathrm{O}(\eta)$ criterion and is comparable to past spectral resolutions listed in Table 1 of Moin and Mahesh (1998).

As will be discussed, despite our high resolution, slight Gibbs ringing is intermittently observed at the smallest scales in the simulation, indicating that viscous dissipation is not entirely resolved (Lecoanet et al. 2016). To quantify the impact of this ringing, in addition to probing the sensitivity of our results to the domain size, we run a second simulation in a cubic domain with side length 4 and $N = 384$ modes, such that $\Delta x = \Delta y \approx 2\eta$. As shown in the appendix, no Gibbs ringing is apparent in this smaller simulation, and the time averages of the velocity field and plume radius in the larger domain and smaller domain agree to within 10% – an uncertainty factor that we will apply to our main results.

We employ the 2nd-order BDF scheme of Wang and Ruuth (2008) to solve the non-linear terms explicitly and the linear terms implicitly with a variable time step set by the Courant-Friedrichs-Lewy condition with a 0.25 safety factor. To achieve a steady state, we employ damping far from the source. Let $C(\hat{x}, \hat{y}, \hat{z})$ be a spatially-varying damping coefficient. Rayleigh drag ($-C\mathbf{u}$) and Newtonian cooling ($-Cb$) are then added to the momentum equation (Eqn. 12) and buoyancy equation (Eqn. 13), respectively. Damping is performed outside of a half ellipse centered at the surface with a vertical semi-major axis of 8 and a horizontal semi-minor axis of 4. A tanh function smoothly damps outside this ellipse:

$$C(\hat{x}, \hat{y}, \hat{z}) = \frac{1+\tanh\left(\frac{f(\hat{x},\hat{y},\hat{z})-H}{\Delta}\right)}{2\hat{\tau}_{\mathrm{damp}}}, \qquad (18)$$

$$f(\hat{x}, \hat{y}, \hat{z}) = \sqrt{2(\hat{x}^2+\hat{y}^2)+\hat{z}^2}, \qquad (19)$$

and we set the damping height as $H = 8$, transition length $\Delta = 1$, and time scale as $\hat{\tau}_{\mathrm{damp}} = 1.5$. Simulations are initialized from rest with small-scale noise added to the starting buoyancy field (of magnitude $\hat{b} \sim 10^{-4}$) to break symmetry. The simulation is run for 40 time units. A statistical steady state is reached at $\hat{t} \approx 10$, and all analysis is performed on the last 30 time units of the simulation. Figure 1 plots instantaneous and time-averaged fields for this simulation.

In contrast to Plourde et al. (2008), no continuous source of artificial noise is needed in the simulations to coax the flow into turbulence. We note that Plourde et al. (2008) reports a diameter-based Reynolds number of 7700, which, upon converting to the radius-based definition (Eqn. 15) used here, yields Re ≈ 3055. Prior experiments with Re ∼ 1000 appear turbulent (as reviewed in Table 1) so the observation in Plourde et al. (2008) of a laminar plume at Re ≈ 3055 is surprising. Plourde et al. (2008) view this laminarity as unrealistic, and the following analysis suggests that this laminarity may be due to under-resolving the flow.

The Kolmogorov length for Re ≈ 3055 is $\eta/R = Re^{-3/4} \approx 1/400$. Plourde et al. (2008) simulated a 10R x 10R x 16R domain on a Cartesian grid with 720 x 720 x 1200 points and uniform spacing in each dimension, yielding $\Delta x = \Delta y = \Delta z \approx 5\eta$. While this is comparable to the resolution used here, Plourde et al. (2008) employ a second-order central difference scheme rather than a spectral method, and finite differences generate significant numerical error. In particular, second-order central difference schemes with $\Delta x = 5\eta$ differentiate a wave with wavelength λ at 95% accuracy only if $\lambda \geq 57\eta$ (Moin and Mahesh 1998). This analysis suggests that significant numerical error is present at inertial scales in Plourde et al. (2008) — consistent with their "unrealistically laminar" observation. Dedalus simulations run with fewer modes than the DNS requirement

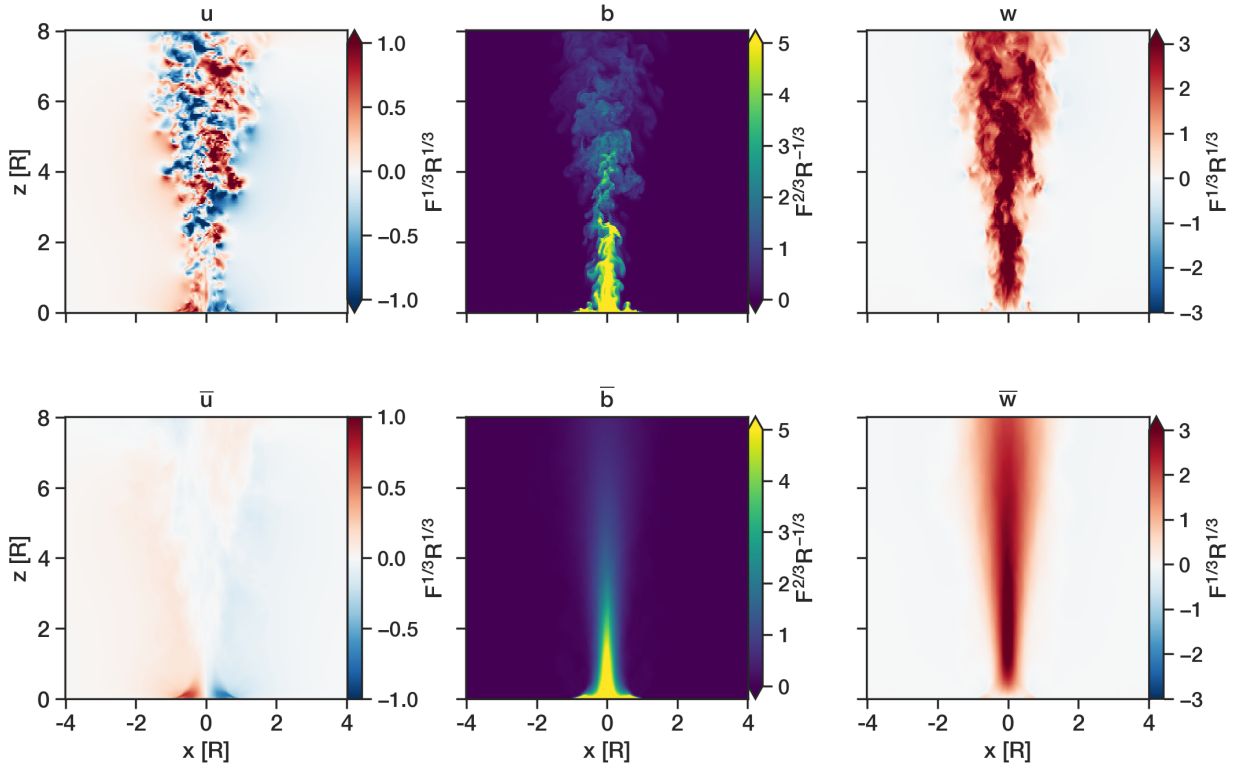

FIG. 1. Instantaneous (top row) and time-averaged (bottom row) cross-sections of a three-dimensional turbulent plume with a Reynolds number of Re = 10^3 and Prandtl number of Pr = .7. Variables are non-dimensionalized in terms of the surface buoyancy source's radius R and magnitude F (with units of velocity × buoyancy).

also appear more laminar in the sense that sharp gradients yield Gibbs waves rather than small-scale turbulent mixing. The result is a narrower plume with less turbulent entrainment (not shown here).

4. Results

We analyze here the results of the two-dimensional (2D) and three-dimensional (3D) DNS of a steady-state, turbulent plume sustained by a circular source of buoyancy at a no-slip surface in an unstratified, unsheared Boussinesq fluid.

a. 2D simulations

The set of two-dimensional simulations (see Table 2) is designed to probe the sensitivity of z_v to a range of Re, varying from laminar to highly turbulent. These simulations are governed by the two-dimensional version of equations 12, 13, and 14 with a surface buoyancy source applied inside of $\hat{x} = 1$ (or inside $x = R$ with dimensional variables). First, we note that the two-dimensional analogues to the MTT equations (Eqn. 4, 5, 6) are

$$\frac{d}{dz}(rw) = \alpha w, \tag{20}$$

$$\frac{d}{dz}\left(rw^2\right) = rb, \tag{21}$$

$$rwb = Q = \text{constant}. \tag{22}$$

The solution with a point source of buoyancy at $r = 0$ and $z = z_v$ is $r = \alpha(z - z_v)$, $b \propto (z - z_v)^{-1}$, and w constant. To diagnose the simulated $r(z)$, we must confront the reality that plumes are not horizontally uniform like the bulk-plume (or top-hat) solution of MTT. Therefore, a functional definition of the plume's radius is required. Following convention (Morton et al. 1956; Kaye and Hunt 2009; Bouzinaoui et al. 2007), we model the plume's radial distribution with a Gaussian. (In the next section, we verify this assumption and plot the Gaussian fit to the 3D data.) At each height, we fit a Gaussian to the time-averaged vertical velocity using least squares and identify the plume's effective radius as $r(z) = \sqrt{2\sigma(z)}$, where σ is the Gaussian's standard deviation. We can then approximate the time-averaged vertical velocity as

$$w(x, z) = w_c(z)e^{-x^2/r(z)^2}, \tag{23}$$

Re	N modes	α	z_v [R]
10^2	256	N/A	N/A
5×10^2	384	.20	−0.94
10^3	512	.24	−0.30
10^4	1024	.24	−0.24

TABLE 2. Set of two-dimensional simulations performed. No z_v is fit to the Re = 10^2 case: this laminar plume grows diffusively and does not exhibit an MTT cone as shown in Figure 2.

where $w_c(z)$ is the time-averaged center-line vertical velocity. The inferred $r(z)$ and center-line fields are plotted in Figure 2, and demonstrate a convergence towards a high-Re limit.

The values of α and z_v given in Table 2 are computed by a linear fit to the $r(z)$ curves far from surface. Given $\alpha = 0.24$, we also estimate the implied virtual origin of the ad hoc spun-up-at-surface assumption by solving for the z_v that enforces $r(0) = R$; that would yield $z_v = -4.12$R. Comparing this prediction to the results in Table 2, we reach two conclusions: 1. the high-Re plume spins up with a virtual origin that is an order of magnitude closer to the surface than in the spun-up-at-surface prediction, and 2. even for Re not yet converged to the high-Re limit, the spun-up-at-surface condition grossly overestimates the proper z_v. We emphasize this last point because the computational constraints of three-dimensional simulations prohibits us from probing a wide range of Re and formally demonstrating Re convergence in three dimensions. The two-dimensional analysis thus lends support to the notion that a Re = 10^3 simulation can be used to assess the accuracy of the spun-up-at-surface assumption in three dimensions.

b. 3D simulations

In three dimensions, 10^3 was the highest achievable Reynolds number given the available computational resources, so a simulation with that Re is the one presented here. We identify $r(z)$ by again following the convention of fitting a Gaussian distribution to the plume's velocity field,

$$w(s,z) = w_c(z)e^{-s^2/r(z)^2}, \tag{24}$$

where $s = \sqrt{x^2+y^2}$ and $w_c(z)$ is the center-line vertical velocity. Figure 3 evinces the goodness of fit. In the left panel of Figure 4, we plot $r(z)$, which, regressed against z, yields an estimate of α and z_v via Eqn. 4. The regression is computed over $z = [3,6]$, over which $r(z)$ appears approximately linear, providing $\alpha = .091 \pm .003$, in close agreement with prior studies (Morton et al. 1956; Carazzo et al. 2006), and $z_v = -(1.14 \pm .02)R$. The uncertainties given here are those stemming from the uncertainty of the least-squares fit.

Since we are not able to run the three-dimensional simulation over a wide range of Reynolds numbers, it is not possible to give a rigorous estimate of the deviation of $z_v = -1.14R$ from the true value of z_v in the high-Reynolds limit. By running a smaller domain and higher resolution simulation, we show in the appendix that the time-averaged velocity and radius have a roughly 10% sensitivity to the domain size and number of modes. In light of this sensitivity, we will quote the result to the closest tenth of R, i.e., $z_v = -1.1$R.

For context, we may get some sense for the Re dependence by looking at the 2D simulations, in which $|z_v|$ decreased by 20% from a Reynolds number of 10^3 to 10^4. If 3D scales identically to 2D, we might expect the high-Re z_v to be slightly closer to the surface than the simulation presented here (run at a Reynolds number of 10^3).

For comparison, the practice of assuming an MTT plume that is spun-up at the surface yields $z_v = -5R/(6\alpha) = -9.2R$. The 3D simulation reveals that this estimate is off by nearly an order of magnitude. The consequences of this disagreement will be explored in the subsequent section. Encouragingly, our finding of $z_v = -1.1$R lies within the range $z_v = [-.86, -2.2]$ identified in past experiments (Table 1). Note that we caution direct comparison, however, because these prior plumes are distinct from the case studied here, as they possessed either a laminar boundary layer, surface volume sources, or a free-slip boundary condition. Comparing to prior theoretical estimates, our result lies closer to the $z_v = 0$ prediction by Hunt and Kaye (2001) (obtained assuming a constant α all the way down to the surface) than to the $z_v = -3.34R$ prediction by Ciriello and Hunt (2020) (obtained using an α that is linear in the Richardson number).

Beyond z_v, we seek a theoretical prediction of the plume's vertical velocity and buoyancy. Formulating conservation equations for the Gaussian plume requires a slight generalization to account for the narrower buoyancy distribution, clearly visible in Figure 1 and 3. Readers are directed to section 1.2 of Hunt and Kaye (2001) for a review of past experimental work on this topic. While the radial distribution of velocity and buoyancy are both shaped by entrainment, we might expect vertical velocity to have a slightly different distribution due to the effects of pressure forces.

To account for buoyancy's narrower profile, we follow the standard practice reviewed in Turner (1986) of introducing a parameter λ such that

$$b(s,z) = b_c(z)e^{-s^2/\lambda^2 r(z)^2}. \tag{25}$$

By least-squares estimation, we find $\lambda = .89 \pm .07$ (compare to $\lambda = .83$ as reported in Bouzinaoui et al. 2007). Now that we have velocity and buoyancy distributions, we can integrate over them to find the MTT conservation equations

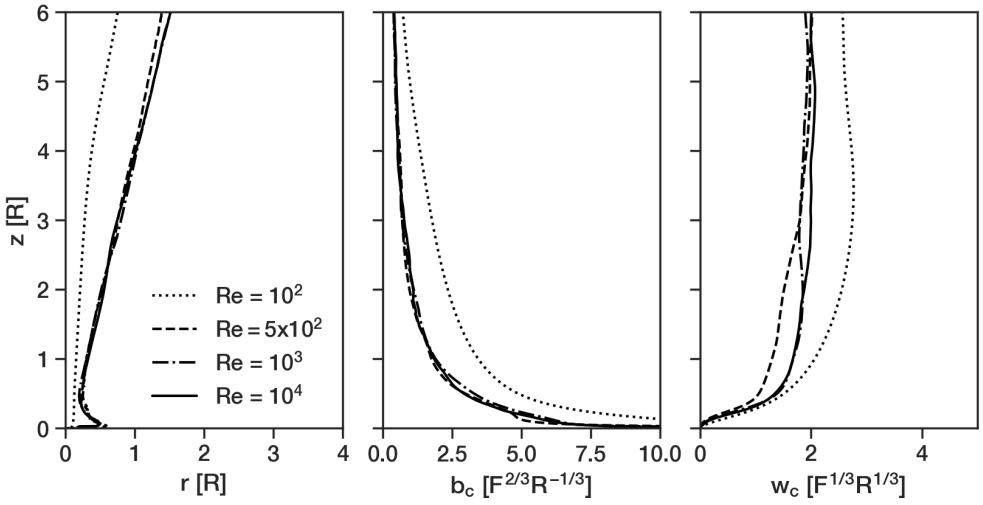

FIG. 2. Time-averaged profiles of two-dimensional plumes with varying Re. The profiles of (left) radius, (middle) axial buoyancy, and (right) axial vertical velocity show a convergence toward an asymptotic turbulent limit.

for a Gaussian plume (Bouzinaoui et al. 2007):

$$\frac{d(w_c r^2)}{dz} = 2\alpha r w_c, \tag{26}$$

$$\frac{d(\frac{1}{2}w_c^2 r^2)}{dz} = \lambda^2 b_c r^2, \tag{27}$$

$$\frac{\lambda^2}{\lambda^2+1} w_c b_c r^2 = Q, \tag{28}$$

which admit the solution,

$$r(z) = \frac{6\alpha}{5}(z - z_v), \tag{29}$$

$$w_c(z) = w_0 Q^{1/3}(z - z_v)^{-1/3}, \tag{30}$$

$$b_c(z) = b_0 Q^{2/3}(z - z_v)^{-5/3}, \tag{31}$$

where we have defined,

$$w_0 = \left(\frac{6\alpha}{5}\right)^{-2/3}\left(\frac{3(\lambda^2+1)}{2}\right)^{1/3}, \tag{32}$$

$$b_0 = \left(\frac{2}{3\lambda^2}\right)\left(\frac{6\alpha}{5}\right)^{-4/3}\left(\frac{3(\lambda^2+1)}{2}\right)^{2/3}. \tag{33}$$

Given the best-fit parameters collected in Table 3, we proceed to computing $w_c(z)$ and $b_c(z)$ as shown in Figure 4. Beneath $z \approx 2R$, the plume fields substantially diverge from the MTT scalings: the vertical velocity goes to zero to match the no-flux surface boundary condition, and the buoyancy field transitions to a conductive layer near the surface. This behavior is manifestly different from the near-surface MTT scalings plotted in dashed lines in Figure 4. Above this surface layer, however, the MTT theory

	b_0	w_0	α	λ	z_v [R]
Central Est.	31.29	6.08	.091	.89	−1.14
Uncert.	3.64	.15	.0003	.073	.02

TABLE 3. Best-fit parameters to Gaussian model of three-dimensional plume.

z [R]	r [R]	b_c [$F^{2/3}R^{-1/3}$]	w_c [$F^{1/3}R^{1/3}$]
0	.68	24.38	0.0
.25	.4	8.22	1.29
.5	.36	7.36	2.19
.75	.33	6.88	2.76
1.0	.32	6.38	3.18
1.25	.32	5.79	3.45
1.5	.33	5.21	3.63
1.75	.34	4.63	3.69
2.0	.35	4.09	3.71

TABLE 4. The high-Re DNS solution for the spin-up of the MTT plume plotted in Figure 4.

is accurate to within 10%, and can be readily employed to estimate the plume's properties. We note that results presented here are non-dimensional and are thus applicable to arbitrary radius R and buoyancy flux F. Numerical values of r, b_c, and w_c at heights below $2R$ are given in Table 4. Taken in combination with the MTT solution constrained by the parameters in Table 3, this amounts to a general and comprehensive description of all sufficiently turbulent Boussinesq plumes rising above uniform circular sources of buoyancy.

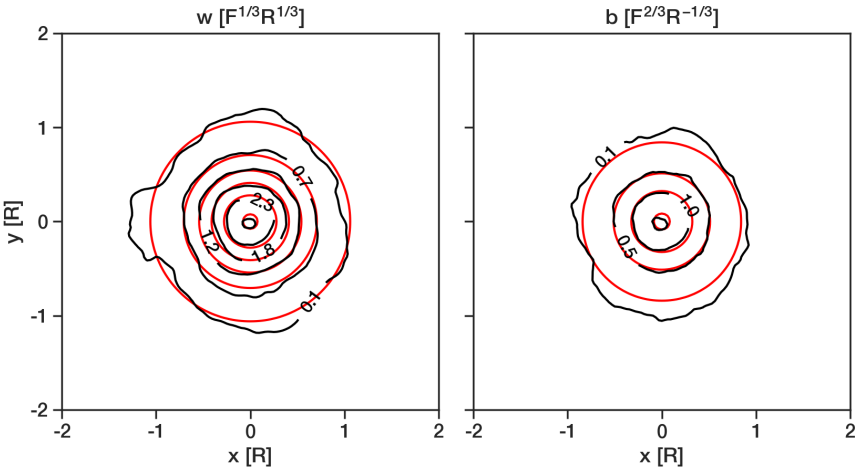

FIG. 3. Horizontal distribution of time-averaged vertical velocity (left) and buoyancy (right) at $\hat{z} = 5$ in the $\mathrm{Re} = 10^3$ simulation (black) and the corresponding least-squares fit (red) to the Gaussian distributions in Eqn. 25.

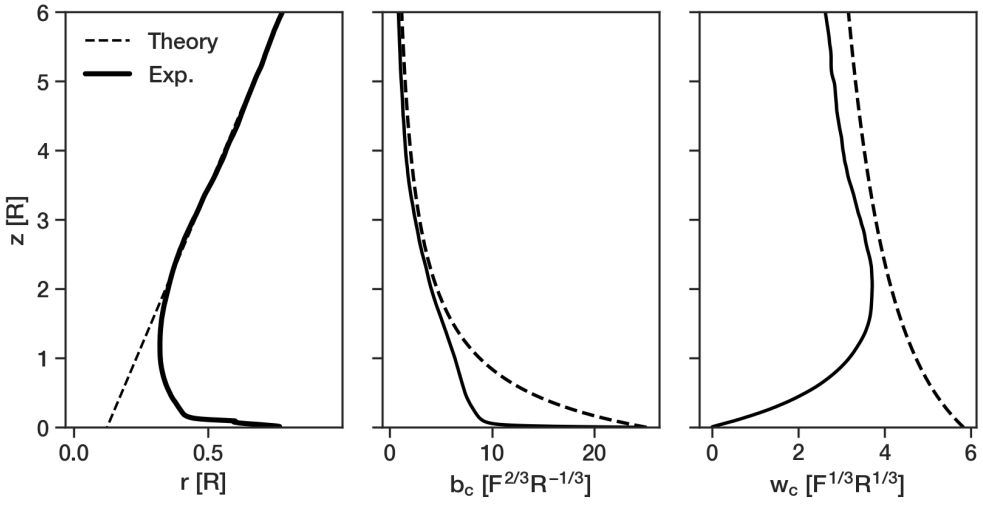

FIG. 4. Time-averaged profiles from (solid) the simulations and (dashed) equations (29-31) of (left) the plume's radius, (middle) axial vertical velocity, and (right) axial buoyancy.

5. Hiroshima fire plume

We are now in a position to calculate the errors generated by the ad hoc closures of 1. placing the virtual origin at the surface (i.e., $z_v = 0$) and 2. assuming the MTT plume is spun-up at the surface with a width equal to that of the buoyancy source (i.e., $z_v = -5R/(6\alpha) = -9.2$). Noting that the numerical solution asymptotes to an MTT solution at about $z = 2R$, we can compare the predictions that those closures would make for the center-line buoyancy at $z = 2R$ relative to the actual buoyancy. Noting that $b_c(z, z_v) \propto (z - z_v)^{-5/3}$, we find

$$\frac{b_c(z = 2R, z_v = 0)}{b_c(z = 2R, z_v = -1.1R)} = \left(\frac{2}{2 + 1.1}\right)^{-5/3} = 2.0 \qquad (34)$$

$$\frac{b_c(z = 2R, z_v = -9.2R)}{b_c(z = 2R, z_v = -1.1R)} = \left(\frac{2 + 9.2}{2 + 1.1}\right)^{-5/3} = 0.12\,. \qquad (35)$$

In other words, the two previously used closures overestimate and underestimate the plume buoyancy by factors of 2.0 and 0.12, respectively.

In the atmosphere, we are often most interested in a plume's level of neutral buoyancy since that determines the height of the layer of concentrated smoke, ash, or other pollutants. For a buoyant plume in an unstratified fluid,

however, there is no level of neutral buoyancy: the plume remains more buoyant than its surroundings at all heights. Thus, the MTT theory – and the closure provided for it in Table 3 – is not directly applicable to plumes outside of a well-mixed layer. On the other hand, we expect that plumes are largely unaffected by environmental stratifications $|\partial b_{\text{env}}/\partial z|$ that are small compared to the plume's own buoyancy gradient $|db_c/dz|$. Therefore, the high-Re solution given in Figure 4 and Table 4 should apply to plumes in a stratified atmosphere near the surface. For this reason, it is likely that the virtual origin of a plume in Earth's stratified atmosphere is nearly identical to the value of $-1.1R$ found here.

Away from the surface, the solution asymptotes to an MTT plume, which is highly constrained by dimensional analysis. By Equation 1, the MTT solution is simply a plume of volume rate $V = \pi r^2 w$. Therefore, the fractional entrainment rate ε for the MTT solution is $\varepsilon \equiv d\log V/dz = (2/r)dr/dz = 2\alpha/r$, where $2\alpha \approx 0.2$. As mentioned earlier, this $1/r$ scaling stems from the reasonable assumption that the eddies responsible for entrainment scale with the size of the plume. Indeed, such $1/r$ scaling has been observed in many other contexts as well, including clouds (Stirling and Stratton 2012) and isolated thermals (Lecoanet and Jeevanjee 2019). Below $z = 2R$, ε deviates from this simple $1/r$ scaling, but its value can be calculated at each height from the evolution of the center-line buoyancy (see below), allowing for the calculation of the full profile of $\varepsilon(z)$.

We can approximate a plume in a stratified atmosphere using the initial conditions and the $\varepsilon(z)$ from the simulation of the unstratified case. For the initial conditions, we take the buoyancy and vertical velocity of the DNS solution at the surface. For adiabatic ascent without entrainment, the dry static energy DSE (equal to $c_pT + gz$) of a lifted parcel is approximately conserved [1]. Parameterizing entrainment as a relaxation of the plume's DSE to the environmental value over the mixing length $1/\epsilon$ yields

$$\frac{d\text{DSE}}{dz} = \varepsilon(\text{DSE}_e - \text{DSE}), \tag{37}$$

where the subscript e denotes environmental values. In addition, we solve an analogous equation for the water-vapor mass fraction q_v to ensure that the solution is terminated when the plume begins to condense:

$$\frac{dq_v}{dz} = \varepsilon(q_{ve} - q_v)\,. \tag{38}$$

[1]DSE - CAPE is the true conserved variable for a lifted adiabatic dry parcel (Romps 2015). Consider ascent over a height H with characteristic buoyancy B. Comparing CAPE $\sim BH$ and the DSE anomaly DSE$' \sim c_pBT_e/g$, we find

$$\frac{\text{CAPE}}{\text{DSE'}} \sim \frac{gH}{c_pT_e} \sim 10^{-1}, \tag{36}$$

where we have plugged in with $H = 10$ km. We therefore take DSE' to be approximately conserved.

While follow-up research is warranted to quantify the impact of stratification on plume solutions, the point we wish to make is in no way subtle, and so this approach will suffice.

In particular, we wish to assess the appropriateness of the spun-up-at-surface approximation in application to the Hiroshima firestorm of August 6, 1945. Well after the mushroom cloud from the nuclear detonation had dissipated, the citywide fire sourced a steady plume of radioactive soot. The fate of soot from such storms is of great practical importance considering the potential for deposition of radioactive material far from the blast site and the potential for soot to enter the stratosphere where it can perturb Earth's climate. To model the fate of that soot, however, it is critical to know the plume's level of neutral buoyancy.

For the Hiroshima firestorm, historical estimates give $R \approx 1$ km and a surface heat flux of 20 kW/m^2 (Aoyama et al. 2011), yielding a buoyancy flux of

$$F = \frac{g}{\rho c_p \theta_0}(20\text{ kW m}^{-2}) \approx 0.7\text{ m}^2\text{ s}^{-3}, \tag{39}$$

where we have let $\theta_0 \approx 300$ K, $\rho \approx 1$ kg m^{-3}, and $c_p \approx 1000$ J kg^{-1} K^{-1}. To make contact with the DNS results, we compute the dimensionful scale $T = F^{-1/3}R^{2/3} \approx 100$ s. In roughly $10T \approx 20$ minutes, the plume ascends from the surface to near the domain top at 10R = 10 km and the simulation achieves steady-state. A steady-state treatment of the Hiroshima plume appears reasonable given that observations show that the firestorm burned for several hours (Aoyama et al. 2011). The velocity scale of the bulk plume is $U = F^{1/3}R^{1/3} \approx 9$ ms^{-1} with max vertical velocities of $w_c \approx 4U \approx 40$ ms^{-1} occurring near 2 km as shown in Figure 4. Axial buoyancies in the mature plume are in excess of the buoyancy scale $B = F^{2/3}R^{-1/3} \approx .07$ ms^{-2}, but share the same order of magnitude above the first hundred meters.

Following the analysis in Tajima (1983), we employ the sounding of Tokyo reported in Kerr et al. (1983) as a proxy for Hiroshima's atmosphere on the morning of August 6, 1945. The sounding, plotted as circles in Figure 5, is consistent with qualitative observations describing "Japan [as] widely covered homogeneously by a hot and humid maritime air mass" (Tajima 1983). We fit third-degree polynomials to these soundings, shown as solid curves in Figure 5.

To predict the fire plume's level of neutral buoyancy, we can model the plume as an MTT plume spun-up at the surface (which we will denote by a subscript "MTT") or we can model the plume using the solution found in the previous section (which we will denote by a subscript "DNS"). As we will see momentarily, the initial conditions and the entrainment profiles differ dramatically between these two cases.

Using equations (29), (31), and (33), we can calculate the initial centerline buoyancy for the spun-up-at-surface

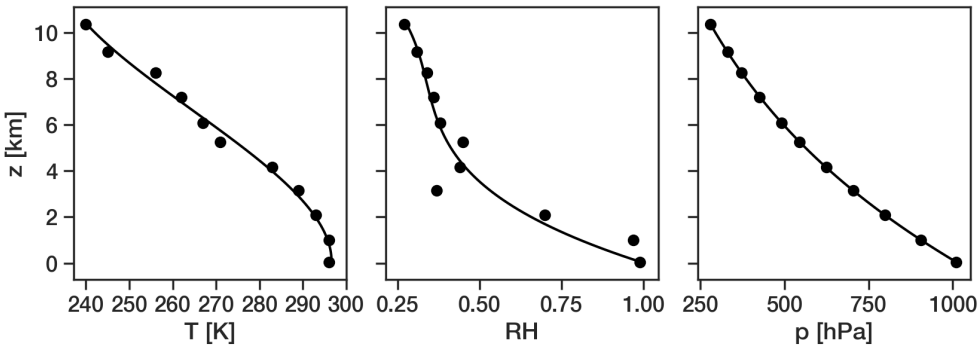

FIG. 5. Hiroshima atmospheric state: temperature, relative humidity, and pressure as estimated from the atmospheric sounding of Tokyo on August 6 at 6:00am local (21:00 UCT, August 5) measured by US strategic bombing command (Kerr et al. 1983). Circles show the sounding and the curves show third-degree polynomial fits.

MTT solution as

$$b_{c,\mathrm{MTT}}(0) = \left(\frac{2}{3\lambda^2}\right)\left(\frac{6\alpha}{5}\right)^{1/3}\left(\frac{3(\lambda^2+1)}{2}\right)^{2/3} Q^{2/3}R^{-5/3} = 0.06 \text{ m s}^{-2}, \quad (40)$$

where the values of α and λ are taken from Table (3), and $Q = FR^2 = 7\times10^5$ m^4 s^{-3}. Note that a buoyancy of 0.06 m s^{-2} corresponds to a temperature anomaly of 2 K. The fractional entrainment rate ε can be found from the dilution of the centerline buoyancy,

$$\varepsilon_{\mathrm{MTT}}(z) = -\frac{d\log b_{c,\mathrm{MTT}}(z)}{dz} = \frac{5}{5R/2\alpha + 3z}. \quad (41)$$

This entrainment rate is plotted in red in the left panel of Figure 6. At the surface, this fractional entrainment rate equals 0.2 km^{-1}.

For the DNS plume, the time-averaged surface buoyancy at the center is

$$b_{c,\mathrm{DNS}}(0) = 24.38F^{2/3}R^{-1/3} = 2 \text{ m s}^{-2}, \quad (42)$$

which corresponds to a temperature anomaly of 60 K. The fractional entrainment rate can be found from the dilution of the centerline buoyancy,

$$\varepsilon_{\mathrm{DNS}}(z) = -\frac{d\log b_{c,\mathrm{DNS}}(z)}{dz}. \quad (43)$$

This is plotted as the black curve in the left panel of Figure 6. Very close to the surface, where conduction is dominant, this is not technically the entrainment rate. In fact, at the surface, this definition gives $\varepsilon_{\mathrm{DNS}}(0) = F/\kappa/b_{c,\mathrm{DNS}}(0)$, which represents pure conduction. Above the non-dimensional height where $\hat{b}\hat{w} = \mathrm{Re}^{-1}\mathrm{Pr}^{-1}d\hat{b}/d\hat{z}$, advection of buoyancy dominates over conduction. For the DNS solution, this occurs at a height of .015; well above this height, it is correct to interpret the $\varepsilon_{\mathrm{DNS}}$ defined in equation (43) as the fractional entrainment rate.

We can integrate the buoyancy (initialized to its surface MTT or DNS value) and water-vapor mass fraction (initialized to the environmental value) using equations (37) and (38), the MTT and DNS entrainment rates in equations (41) and (43), respectively, and the polynomial fits to the soundings for the environmental values of DSE and q_v. The resulting profiles of buoyancy for the MTT and DNS plumes are plotted in the middle panel of Figure 6 up to their lifting condensation levels (LCLs). As a result of the stable conditions and the MTT parcel's unremarkable buoyancy, the lifting calculation pegs the spun-up-at-surface MTT LCL to within 100 m of the surface. Given the environmental convective inhibition (CIN), we conclude that the spun-up-at-surface plume will not reach the upper atmosphere. In contrast, the DNS parcel achieves an LCL of roughly 2 km. Will the DNS parcel reach the upper atmosphere? CIN above the LCL complicates the answer, which depends on the parcel's momentum and moist ascent. A naive estimate of $w_{\mathrm{LCL}} = (2\int b\,dz)^{1/2} \approx 30$ m/s suggests that the parcel may overcome the overlying CIN ≈ 100 J/kg even without additional buoyancy from latent heating. Regardless, the DNS parcel's trajectory is markedly different than the spun-up-at-surface MTT parcel, which would predict that all of Hiroshima's hot gases and radioactive soot would remain trapped near the surface. For comparison, computer vision analysis of Hiroshima firestorm photographs suggests that the plume extended up to a height of 16 km (Baba et al. 2011). Lifting the parcel beyond the LCL and comparing the moist level of neutral buoyancy to this observation requires an account of moist entrainment and microphysics, which is beyond the scope of this paper.

6. Conclusion

Turbulent plumes (sustained by a circular source of buoyancy at a no-slip lower boundary in an unsheared, unstratified fluid) exhibit a distinct spin-up stage before they transition to the scalings predicted by Morton et al.

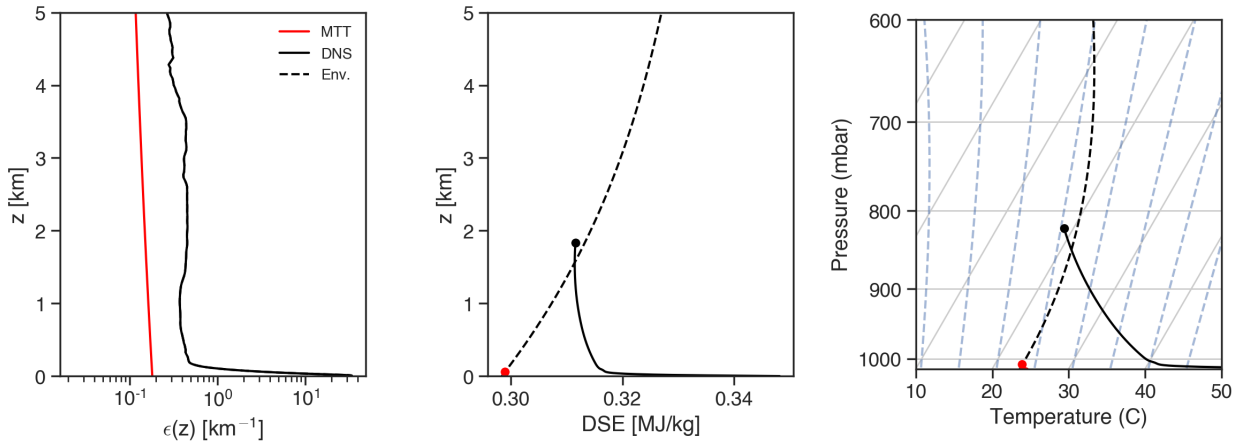

FIG. 6. (left) Fractional entrainment rate ε for the (red) spun-up-at-surface MTT (red) and (black) DNS solutions. (middle) Profiles of buoyancy up to the lifting condensation level (marked by a circle) using the initial conditions and entrainment rates appropriate to the spun-up-at-surface MTT and DNS cases. (right) Skew-T log-p diagram of the (dashed) environment and (solid) parcel trajectories.

(1956, MTT). Two facts – the rapid convergence of solutions to the high-Re limit and the approximate invariance of plume solutions with respect to the Prandtl number – lead to a remarkable simplification of the solution set of turbulent plumes. Indeed, postulating invariance with respect to both Re and Pr in the high-Re limit, there are no remaining free parameters. This suggests that the DNS solution presented here (see Figure 4) is the one and only solution for all such turbulent plumes. Although we have presented evidence from two-dimensional solutions that this three-dimensional simulation is plausibly converged to the high-Re limit at a Reynolds number of only 10^3, simulations or experiments at higher Reynolds numbers should be performed to confirm this.

Well above the surface, all plumes (in an unstratified, unsheared fluid) asymptote to the MTT solutions. Since the ratio of the entrainment velocity to the updraft speed (α) rapidly converges to about 0.1 in the high-Reynolds limit, the dimensional MTT solutions are uniquely defined by only two parameters: the buoyancy source rate Q and the height of the virtual origin z_v. Since Q is typically a given, this leaves only z_v to be determined.

The three-dimensional DNS solution obtained here establishes that the plume's virtual origin is substantially different from the values previously used. Previous work has often assumed that the plume is spun up to an MTT solution at the surface with a width equal to the width of the buoyancy source. That spun-up-at-surface assumption places the virtual origin of the MTT plume below the surface a distance about ten times the radius of the buoyancy source. In contrast, the DNS solution finds a virtual origin that lies below the surface by a distance equal to 1.1 times the source radius (see Table 3). Consequently, the spun-up-at-surface approximation implies a buoyancy at a height of $2R$ (which is where the DNS solution asymptotes to the MTT solution) that is 10 times too small (see equation 35).

We have applied the DNS solution to the case of the Hiroshima firestorm to predict the level of neutral buoyancy of the generated plume. The spun-up-at-surface approximation would predict that the radioactive soot would be trapped within a few hundred of meters of the surface. In contrast, using the entrainment rate obtained from the DNS solution, we predict that the plume reached the free troposphere, and possibly even the upper atmosphere (Figure 6) in agreement with observational evidence (Baba et al. 2011).

The last result is of particular importance because soot in the upper atmosphere — suspended above the weather layer — may remain aloft for months to years. Spread across the globe by the stratospheric circulation, this upper atmospheric soot can produce substantial surface cooling. In the nuclear firestorm context, this cooling may induce a so-called nuclear winter (see, e.g., Toon et al. 2007). Thus, an accurate estimate of the plume's virtual origin is essential to predicting the plume's upper-atmospheric fate.

Acknowledgments. This work was supported by the National Science Foundation under grant 2127071. The authors thank three anonymous reviewers for helpful comments and Nadir Jeevanjee for pointing out an erroneous factor of π in an earlier draft of the manuscript.

7. Appendix

Here we describe a smaller-domain simulation run to assess the impact of the slight Gibbs ringing and domain-size effects in the larger three-dimensional simulation described in Section 3. We employ a cubic domain of side length $4R$ with $N = 384$ modes (compare to the 12R length and $N = 512$ modes of the larger simulation). At the same Re

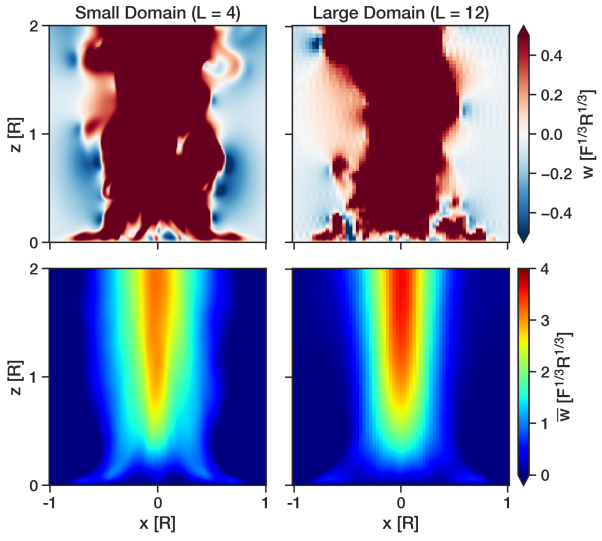

FIG. 7. Top row: near-source instantaneous vertical velocity in the small domain (left) and large domain (right). Large domain data is a subregion of Figure 1 plotted with a color scheme that highlights the wave-like ringing rather than the mean fields. Bottom row: comparison of the time-averaged vertical velocities. See text for discussion.

of 10^3, the smaller domain has $\Delta x = 2\eta$ while the larger simulation has $\Delta x = 4\eta$. All other aspects of the numerical setup are the same except for the damping layer, which is described by equation 19 but with a smaller height $H = 2.5$, transition length $\Delta = .25$, and $\tau_{\text{damp}} = 1/3$. The simulation is run for 20T and time averages are performed over the last 10T to compute the mean fields.

Figure 7 compares this smaller domain simulation to the larger simulation. The same larger simulation data plotted in Figure 1 is shown again in Figure 7, but with a different color scheme that emphasizes the slight ringing — an order of magnitude smaller than the mean fields. Thanks to the exponentially fast convergence of spectral DNS (Lecoanet et al. 2016), increasing the resolution eliminates any visible signs of Gibbs ringing, indicating that the small domain simulation is well converged. The bulk geometry of the plumes and the magnitudes of the vertical velocity are in broad agreement between the two simulations. The larger domain simulation, however, exhibits a roughly 10% higher peak velocity. Both the domain size and resolution are different, so the exact source of this discrepancy is unclear. We leave that question to future work, and, for the purposes of this paper, we take 10% to be a rough estimate of the uncertainty in the larger simulation results.

References

Aoyama, M., N. Kawano, T. Koizumi, and Y. Okada, 2011: *Estimation of heat, water, and black carbon fluxes during the fire induced by the Hiroshima A-bomb*, chap. 5. 978-4-9905935-0-6, Hiroshima City.

Baba, M., F. Ogawa, S. Hiura, and N. Asada, 2011: *Height Estimation of Hiroshima A-bomb Mushroom Cloud from Photos*, chap. 6. 978-4-9905935-0-6, Hiroshima City.

Bouzinaoui, A., R. Devienne, and J. R. Fontaine, 2007: An experimental study of the thermal plume developed above a finite cylindrical heat source to validate the point source model. *Experimental Thermal and Fluid Science*, **31 (7)**, 649 – 659, doi:https://doi.org/10.1016/j.expthermflusci.2006.06.010.

Burns, K. J., G. M. Vasil, J. S. Oishi, D. Lecoanet, and B. P. Brown, 2020: Dedalus: A flexible framework for numerical simulations with spectral methods. *Physical Review Research*, **2 (2)**, 023 068.

Carazzo, G., E. Kaminski, and S. Tait, 2006: The route to self-similarity in turbulent jets and plumes. *Journal of Fluid Mechanics*, **547**, 137.

Carrier, G., F. Fendell, and P. Feldman, 1985: Firestorms. *Defense Nuclear Agency Technical Reports*, **DNA-TR-81-102**.

Ciriello, F. and G. R. Hunt, 2020: Analytical solutions and virtual origin corrections for forced, pure and lazy turbulent plumes based on a universal entrainment function. *Journal of Fluid Mechanics*, **893**, A12, doi:10.1017/jfm.2020.225.

Colomer, J., B. Boubnov, and H. Fernando, 1999: Turbulent convection from isolated sources. *Dynamics of atmospheres and oceans*, **30 (2-4)**, 125–148.

Devenish, B. J., G. G. Rooney, and D. J. Thomsn, 2010: Large-eddy simulation of a buoyant plume in uniform and stably stratified environments. *Journal of Fluid Mechanics*, **652**, 75âĂŞ103, doi:10.1017/S0022112010000017.

Elicer-CortÃĺs, J. C., 1998: Measurement of the temperature field in an axisymmetric thermal pure plume. *Experimental Heat Transfer*, **11 (3)**, 207–219, doi:10.1080/08916159808946562.

Epstein, M. and J. Burelbach, 2001: Vertical mixing above a steady circular source of buoyancy. *International Journal of Heat and Mass Transfer*, **44**, 525–536.

Fontaine, J. R., R. Devienne, and S. Rose, 2006: Numerical simulation and experimental validation of plume flow from a heated disk. *Numerical Heat Transfer, Part A: Applications*, **50 (7)**, 645–666, doi:10.1080/10407780600650720.

Freitas, S. R., K. M. Longo, R. Chatfield, D. Latham, M. A. F. Silva Dias, M. O. Andreae, E. Prins, J. C. Santos, R. Gielow, and J. A. Carvalho Jr., 2007: Including the sub-grid scale plume rise of vegetation fires in low resolution atmospheric transport models. *Atmospheric Chemistry and Physics*, **7 (13)**, 3385–3398, doi:10.5194/acp-7-3385-2007, URL `https://www.atmos-chem-phys.net/7/3385/2007/`.

Friedl, M., C. Härtel, and T. Fannelop, 1999: An experimental study of starting plumes over area sources. *Il nuovo cimento C*, **22 (6)**, 835–846.

Hunt, G. R. and N. G. Kaye, 2001: Virtual origin correction for lazy turbulent plumes. *Journal of Fluid Mechanics*, **435**, 377–396.

Kaye, N. B. and G. R. Hunt, 2009: An experimental study of large area source turbulent plumes. *International Journal of Heat and Fluid Flow*, **30**, 1099–1105.

Kerr, G. D., J. V. Pace, III, and W. H. Scott, Jr., 1983: Tissue kerma vs distance relationships for initial nuclear radiation from the atomic

devices detonated over hiroshima and nagasaki. *ORNL Technical Reports*, doi:10.2172/6259209.

Kofoed, P. and P. V. Nielsen, 1990: Thermal plumes in ventilated rooms: measurements in stratified surroundings and analysis by use of an extrapolation method. *Indoor Environmental Technology*, **14**.

Kuznetsov, E. A., E. V. Kolesnik, and E. F. Khrapunov, 2019: Visualization of instability processes in pure thermal plume. *Journal of Physics: Conference Series*, **1382**, 012 020, doi:10.1088/1742-6596/1382/1/012020.

Lecoanet, D. and N. Jeevanjee, 2019: Entrainment in resolved, dry thermals. *Journal of the Atmospheric Sciences*, **76 (12)**, 3785–3801.

Lecoanet, D., M. McCourt, E. Quataert, K. J. Burns, G. M. Vasil, J. S. Oishi, B. P. Brown, J. M. Stone, and R. M. O'Leary, 2016: A validated non-linear kelvin–helmholtz benchmark for numerical hydrodynamics. *Monthly Notices of the Royal Astronomical Society*, **455 (4)**, 4274–4288.

Mahmoud, A., J. Bouslimi, and R. Maad, 2009: Experimental study of the effects of a thermal plume entrainment mode on the flow structure: Application to fire. *Fire Safety Journal*, **44**, 475–486, doi:10.1016/j.firesaf.2008.10.003.

Manins, P., 1985: Cloud heights and stratospheric injections resulting from a thermonuclear war. *Atmospheric Environment (1967)*, **19 (8)**, 1245–1255.

Moin, P. and K. Mahesh, 1998: Direct numerical simulation: A tool in turbulence research. *Annual Review of Fluid Mechanics*, **30 (1)**, 539–578, doi:10.1146/annurev.fluid.30.1.539.

Morton, B. R., G. I. Taylor, and J. S. Turner, 1956: Turbulent gravitational convection from maintained and instantaneous sources. *Proceedings of the Royal Society of London. Series A. Mathematical and Physical Sciences*, **234 (1196)**, 1–23, doi:10.1098/rspa.1956.0011.

Paugam, R., M. Wooster, S. Freitas, and M. ValÃĆ Martin, 2016: A review of approaches to estimate wildfire plume injection height within large-scale atmospheric chemical transport models. *Atmospheric Chemistry and Physics*, **16 (2)**, 907–925, doi:10.5194/acp-16-907-2016, URL https://www.atmos-chem-phys.net/16/907/2016/.

Penner, J., L. Haselman Jr, and L. Edwards, 1986: Smoke-plume distributions above large-scale fires: Implications for simulations of âĂIJnuclear winterâĂİ. *Journal of Applied Meteorology and Climatology*, **25 (10)**, 1434–1444.

Plourde, F., M. V. Pham, S. D. Kim, and S. Balachandar, 2008: Direct numerical simulations of a rapidly expanding thermal plume: structure and entrainment interaction. *Journal of Fluid Mechanics*, **604**, 99âĂŞ123, doi:10.1017/S0022112008001006.

Popiolek, Z., Z. Trzeciakiewicz, and M. S., 1998: Improvement of a plume volume flux calculation method. *Proceedings of the 6th International Conference on air distribution in rooms – Roomvent*, 423–430.

Romps, D. M., 2015: MSE minus CAPE is the true conserved variable for an adiabatically lifted parcel. *Journal of the Atmospheric Sciences*, **72 (9)**, 3639–3646.

Rooney, G. and P. Linden, 1996: Similarity considerations for non-boussinesq plumes in an unstratified environment. *Journal of fluid mechanics*, **318**, 237–250.

Scorer, R. S., 1957: Experiments on convection of isolated masses of buoyant fluid. *Journal of Fluid Mechanics*, **2 (6)**, 583âĂŞ594, doi:10.1017/S0022112057000397.

Stirling, A. J. and R. A. Stratton, 2012: Entrainment processes in the diurnal cycle of deep convection over land. *Quarterly Journal of the Royal Meteorological Society*.

Tajima, E., 1983: Estimation of the hiroshima bomb yield and weather conditions at the time of the bomb. *Second US-Japan Workshop on Reassessment of Atomic Bomb Radiation Dosimetry*, Radiation Effects Research Foundation.

Toon, O. B., R. P. Turco, A. Robock, C. Bardeen, L. Oman, and G. L. Stenchikov, 2007: Atmospheric effects and societal consequences of regional scale nuclear conflicts and acts of individual nuclear terrorism. *Atmospheric Chemistry and Physics*, **7 (8)**, 1973–2002, doi:10.5194/acp-7-1973-2007, URL https://doi.org/10.5194/acp-7-1973-2007.

Turner, J. S., 1986: Turbulent entrainment: the development of the entrainment assumption, and its application to geophysical flows. *Journal of Fluid Mechanics*, **173**, 431âĂŞ471, doi:10.1017/S0022112086001222.

Vuong Pham, M., F. Plourde, and S. Doan Kim, 2005: Three-dimensional characterization of a pure thermal plume. *Transactions of the ASME*, **127**, 624–636.

Wang, D. and S. J. Ruuth, 2008: Variable step-size implicit-explicit linear multistep methods for time-dependent partial differential equations. *Journal of Computational Mathematics*, 838–855.

Woods, A. W., 2010: Turbulent plumes in nature. *Annual Review of Fluid Mechanics*, **42 (1)**, 391–412, doi:10.1146/annurev-fluid-121108-145430.